

Quantum Logic with Interacting Bosons in 1D

Yoav Lahini^{1,*}, Gregory R. Steinbrecher², Adam D. Bookatz¹, and Dirk Englund²

¹*Department of Physics, Massachusetts Institute of Technology, Cambridge MA, USA and*

²*Research Laboratory of Electronics, Department of Electrical Engineering and Computer Science, Massachusetts Institute of Technology, Cambridge MA, USA*

We present a scheme for implementing high-fidelity quantum logic gates using the quantum walk of a few interacting bosons on a one-dimensional lattice. The gate operation is carried out by a single compact lattice described by a one-dimensional Bose-Hubbard model with only nearest-neighbor hopping and on-site interactions. We find high-fidelity deterministic logic operations for a gate set (including the CNOT gate) that is universal for quantum information processing. We discuss the applicability of this scheme in light of recent developments in controlling and monitoring cold-atoms in optical lattices, as well as an implementation with realistic nonlinear quantum photonic devices.

Introduction — Quantum walks (QWs) are unitary processes that describe the quantum-mechanical analogue of the classical random walk process [1–3]. Since their conception, there has been a broad interest in their possible use for quantum information processing [3, 4]. Two mathematical models for QWs have been developed: the discrete-time QW [1], in which the particle takes discrete steps in a direction given by a dynamic internal degree of freedom (a coin), and the continuous-time QW [2] in which the dynamics are described by Hamiltonian evolution on a lattice in the tight-binding representation. Here, we consider the continuous-time quantum walk on a one-dimensional lattice.

Experimentally, QWs have been implemented with photons [5–12], trapped ions [13, 14], and ultra-cold atoms [15–17], among other platforms. Specifically in the field of ultra-cold atoms [17, 18], the degree of experimental control is remarkable: it is possible to prepare an initial state with single-site and single-particle resolution, to create arbitrary one- or two-dimensional lattice potentials, to determine the interaction between the particles, and to directly monitor in real space the evolving many-body distribution.

The ability to control and monitor quantum particles with such precision offers an interesting route to the implementation of quantum information processing and quantum computation schemes. Universal quantum computation has been theoretically shown possible using QWs with interacting particles on certain non-trivial two-dimensional lattices [19, 20] and on one-dimensional lattices with a large number of degrees of freedom at each lattice site [21–23]. However, an implementation using quantum particles hopping on a simple one-dimensional lattice, without any additional degrees of freedom, is not known. Such a geometry would greatly simplify the experimental implementation, bringing it into the realm of recently reported experimental techniques [17]. Furthermore, one-dimensional implementations offer other important practical advantages, for example freeing the second spatial dimension for important tasks such as error correction or connecting remote qubits. Other important

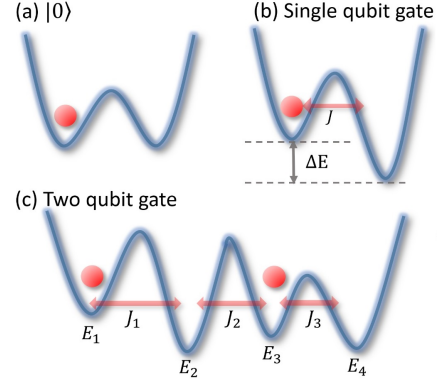


Figure 1: (color online). Illustration of one-dimensional quantum walk based quantum gates. (a) A qubit in the state $|0\rangle$ with dual-rail encoding. (b) Implementation of a single-qubit gate. (c) Schematic of a two-qubit system on a lattice.

tasks such as process tomography could still be performed in 1D (see Supplementary Information).

In this work, we show how it is possible to use multi-particle continuous-time quantum walks in a simple geometry — a one-dimensional lattice with only nearest-neighbor hopping and on-site interactions — as a compact platform for implementing quantum logic. We demonstrate our approach by detailing a set of lattice potentials that yield, with high fidelity, a universal set of quantum gates with only two sites per qubit. Moreover, the required lattice potential for each gate is time-invariant, simplifying the experimental implementation and possibly reducing the total operation time. Thus, high-fidelity gates can be constructed with lower probabilities of qubit-loss errors (i.e. lost particles during the computation) that necessitate computationally costly error-correction procedures. While we focus on interacting ultra-cold bosonic atoms trapped in an optical lattice — a physical system in which our results can be implemented with existing experimental techniques [17] — we also discuss the possibility of extending our analysis to nonlinear quantum photonic systems.

The dynamics of bosonic particles on a lattice is

described by the time-independent many-body Bose-Hubbard Hamiltonian

$$H = \sum_m E_m a_m^\dagger a_m + \sum_{\langle l, m \rangle} J_{l, m} a_l^\dagger a_m + \frac{\Gamma}{2} \sum_m n_m (n_m - 1), \quad (1)$$

where E_m is the on-site energy of site m , $a_m^\dagger \backslash a_m$ is the creation \backslash annihilation operator for a boson in site m , $n_m = a_m^\dagger a_m$ is the number operator, $J_{l, m} \leq 0$ is the tunneling rate between nearest neighbors, and Γ is the on-site interaction energy that arises when two or more bosons occupy the same site. The unitary transformation describing the evolution of multiple quantum particles propagating on the lattice is given by e^{-iHt} , where t is the propagation time. The quantum logic gates discussed here will be implemented by evolving under this Hamiltonian (with a suitable choice of parameters) for some predefined time t_{final} which we take to be $t_{final} = 1$.

Defining qubits on a lattice — The basic element of interest for quantum gates of the type discussed here is the quantum bit, or *qubit*. The continuous-time quantum walk, however, is described by the evolution of quantum particles on a lattice according to the Hamiltonian described in Eq. 1. To define our qubits on the lattice, we use a spatial encoding where a qubit is physically implemented by a single boson in a pair of neighboring potential wells (see Fig. 1), with the states $|0\rangle$ and $|1\rangle$ of the qubit defined by the particle being in the left or right well (i.e. dual-rail encoding). A single quantum particle can occupy the two sites in a superposition, encoding a qubit without the need for additional degrees of freedom. In this way, a system of n qubits can be realized in one dimension with n bosons and $2n$ lattice sites, with one boson in the first two sites (representing the first qubit), one boson in the next two sites (representing the second qubit), and so forth. Note that in this geometry, many physically permitted lattice states (e.g. those with more than one particle on the same site) are not members of the logical space (i.e. the multi-qubit tensor-product space). Nevertheless, we show that it is possible to engineer the lattice parameters such that, at time $t = 1$, $U = e^{-iH}$ maps logical states only to other logical states with high fidelity, even though states outside this subspace are allowed at intermediate times.

Implementing quantum gates — Having defined our qubits, we turn to the task of designing a universal set of quantum gates, i.e. finding lattice parameters that yield desired unitary transformations on the logical space. Designing and building quantum logic gates remains one of the most difficult aspects of quantum computing, and our case is no exception. From the physical description of a given device — in our case, the lattice parameters — it is straightforward to write down the many-particle Hamiltonian and to calculate the unitary evolution operator

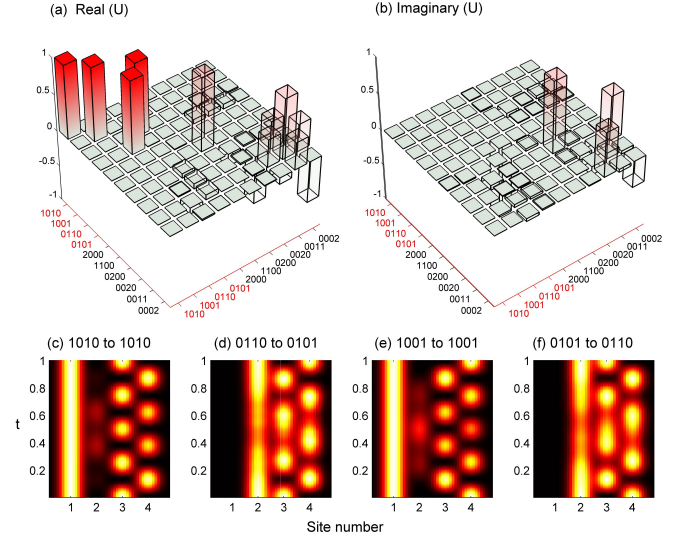


Figure 2: (color online). An implementation of the controlled-NOT (CNOT) gate according to the recipe in Eq. 2. (a) The real part and (b) the imaginary part of the two-particle unitary transform, U . The CNOT gate operation corresponds to the sub-matrix of the logic states, shown in solid-color bars and marked with red axis labels. Plots (c)-(f) show the position (in terms of the lattice sites, 1-4) of the particle density as a function of time, t , revealing the operation principle of the gate on each logical state ($|00\rangle$, $|10\rangle$, $|01\rangle$, and $|11\rangle$ respectively). One observes that the target qubit (in sites 3 & 4) performs Rabi-oscillations that are perturbed by the state of the control qubit (in sites 1 & 2) — the target qubit performs one fewer Rabi-flip if the control qubit is in the $|1\rangle$ state.

$U = e^{-iH}$ that fully describes the operation of the device. The inverse problem, however, is hard: given a desired unitary U , it is difficult to find a corresponding Hamiltonian that meets the physical and geometrical constraints of the device, e.g. the one-dimensionality of the lattice. Furthermore, if the logical quantum states are only a subset of the full Hilbert space, then the quantum gate operation is only a sub-matrix of the overall evolution operator U . In this case, U is not even uniquely defined by the desired gate operation. As described below, we tackle these difficulties with a computational approach that finds appropriate lattice parameters to approximate a given gate operation with high fidelity.

There are many options for the choice of a universal set of gates. One useful choice is the gate set of the controlled-NOT (CNOT) operation, along with either all single-qubit rotations (exactly universal) or the phase-shift gates and the Hadamard gate (approximately universal) [24]. In the following, we elaborate on the construction of the CNOT gate. Single-qubit gates involve only a single particle (i.e. no interaction terms) and are straightforward to calculate, as we detail in the Supplementary Information.

To design the CNOT gate (a two-qubit gate) with the

dual-rail encoding, we consider a lattice with four sites and two bosons. This problem then is defined by eight lattice parameters: four on-site potential terms (E_m in Eq. 1), three tunneling terms ($J_{l,m}$), and the interaction parameter (Γ). The complete two-body Hamiltonian H is described by a 10×10 matrix (the size of the Hilbert space for two bosons in four modes). To perform the logical gate operation, the system is evolved according to $U = e^{-iH}$. The CNOT gate operation is then given by a 4×4 sub-matrix of U over the logical states $|1010\rangle, |1001\rangle, |0110\rangle, |0101\rangle$ (presented here in the occupation number basis); the other six basis states, while physically allowed, are not members of the logical basis.

As explained above, finding the physical lattice parameters from the desired gate is a non-trivial inverse problem. Using non-linear optimization techniques [25–28] (see Supplementary Information), we optimized the eight parameters of the system to maximize the fidelity of the gate when acting on the logical input states under the constraints that the parameters represent a physical one-dimensional lattice, i.e. that the on-site parameters are real, that the tunneling parameters are real and non-positive and connect only nearest-neighboring sites, and that the values of the on-site, tunneling, and interaction terms are within experimentally relevant bounds. Specifically, we demanded that $0 \geq J_{l,m} \geq -J_{max}$, $-J_{max} \geq E_m \geq J_{max}$, and $\Gamma \leq \Gamma_{max}$, where J_{max} and Γ_{max} are the largest allowed tunneling rate and interaction level in the optimization protocol. In our optimization we set $J_{max} = 4\pi$, limiting the maximal number of tunneling events (or Rabi-oscillations) to 4. In practice, this experimental bound is dictated by the loss and decoherence rate of the system, determining the maximal relevant propagation time. We also set $\Gamma_{max} = 10J_{max}$.

An example of a resulting lattice that yields the two-qubit CNOT gate is given (to two decimal places) by

$$G_{CNOT} = \pi \begin{pmatrix} 0.40 & 0 & 0 & 0 \\ 0 & 1.82 & -1.03 & 0 \\ 0 & -1.03 & -0.37 & -3.80 \\ 0 & 0 & -3.80 & -0.66 \end{pmatrix} \quad (2)$$

with interaction strength $\Gamma = 21.68\pi$. Here, the diagonal and off-diagonal entries of G_{CNOT} represent the parameters E_m and $J_{l,m}$, respectively, of the Hamiltonian H . Eq. 2 represents a recipe for a four-site lattice that yields a CNOT gate with fidelity of 99.6%, whose operation is summarized in Fig. 2.

If the bounds on the parameters are relaxed, the fidelity approaches even closer to unity. Fig. 3 summarizes the optimization results. Fig. 3(a) shows the convergence of independent runs with random starting points to the same final result. Fig. 3(b) presents the expected gate fidelity vs. the maximally allowed values of the interaction Γ_{max} . For a fixed maximal tunneling of $J_{max} = 4\pi$, the

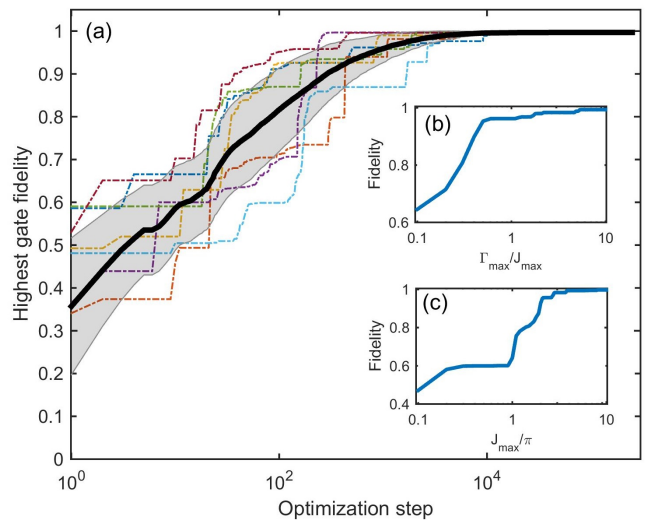


Figure 3: (color online). Optimization of the quantum-walk-based CNOT gate fidelity. (a) Convergence of different optimization runs to the optimal gate fidelity. The solid black line and the shaded area represents the average and the standard deviation values over 512 runs. Seven example runs are shown in the background (dotted lines). (b) Gate fidelity versus the maximum allowed interaction level Γ_{max} , at a constant $J_{max} = 4\pi$. (c) Gate fidelity for different maximal tunneling rates J_{max} at a constant maximal interaction level of $\Gamma_{max} = 20\pi$.

fidelity achieves a value close to 0.95 at $\Gamma_{max}/J_{max} = 0.5$ and then slowly approaches unity as this value is further increased. In a system with a given Γ_{max} , it is still possible to improve the fidelity further by allowing more tunneling events to take place, i.e. increasing J_{max} ; see Fig 3(c).

Compiling a three-qubit primitive — Implementing a quantum algorithm using the scheme presented in this paper will involve several lattice configurations operating in sequence, as gates are sequentially applied in the algorithm. In principle, because the gate set presented in this work is universal, any multi-qubit operation can be broken down into a sequence of single- and two-qubit gates, and thus implemented using the gates already presented. However, compiling common multi-step operations into a single primitive based on a single, time-independent Hamiltonian could reduce the possibility of errors arising from dynamic changes to the lattice. As an example, we constructed a 3-qubit gate, shown in Fig. 4. This gate is useful, for instance, in the 2-bit Deutsch-Jozsa algorithm [29], performing the oracle for the function $f(x, y) = x \oplus y$. (All other oracles for the 2-bit Deutsch-Jozsa algorithm are either a simple variation of this oracle or require only single-qubit gates plus at most one CNOT gate.) Our computational approach allowed us to find a set of lattice parameters that realizes the complete three-qubit operation in a single gate. Fig. 4 presents an implementation of this three-qubit operation, at a fi-

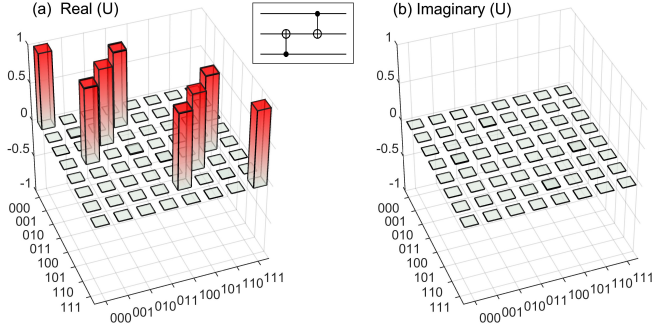


Figure 4: (color online). A 3-qubit operation of 2 CNOT gates (inset), compiled into a single gate U . (a) The real and (b) imaginary parts of our implementation of U . Only the logical basis states are shown.

delity of 99.8%, using a single, one-dimensional six-site lattice:

$$G = \pi \begin{pmatrix} 5.98 & 0 & 0 & 0 & 0 & 0 \\ 0 & 7.13 & -1.21 & 0 & 0 & 0 \\ 0 & -1.21 & 0.14 & -12.04 & 0 & 0 \\ 0 & 0 & -12.04 & 0.18 & -1.37 & 0 \\ 0 & 0 & 0 & -1.37 & 11.69 & 0 \\ 0 & 0 & 0 & 0 & 0 & -8.03 \end{pmatrix} \quad (3)$$

with interaction strength $\Gamma = 108.24\pi$. In this case too, the fidelity could be improved by allowing larger tunneling rates.

Photonic systems — While we have focused our attention on cold atoms, it is possible to extend our scheme to nonlinear photonic systems, for example superconducting circuit QED systems [30] or nonlinear quantum-optical systems [31–37]. First, consider a system described by a similar Hamiltonian to that of Eq. 1: a set of coupled resonators exhibiting a single-photon Kerr nonlinearity [38]

$$H = \sum_m \omega_m \left(a_m^\dagger a_m + \frac{1}{2} \right) + \sum_{\langle l, m \rangle} J_{l, m} a_l^\dagger a_m + \frac{K}{2} \sum_m n_m (n_m - 1), \quad (4)$$

where ω_m is the resonant frequency of the m th cavity and K the strength of the Kerr nonlinearity. Replacing ω_m with E_m and K with Γ , we regain Eq. 1 exactly (neglecting the zero-point offset). Such systems have been experimentally demonstrated [38] and site-by-site tunable coupled-cavity systems have been proposed [39]. However, our scheme requires a different E_m (here, cavity frequency) at each lattice site, which is difficult to reconcile with a high-Q coupled resonant system.

We can remedy this issue by instead coupling each of the cavities to a virtual two-level atom, whose transition

frequency $\omega_{a, m}$ is detuned from the (now constant) cavity resonance ω_c by a frequency $\Delta_m = \omega_{a, m} - \omega_c$. The Hamiltonian is then well described by [40]

$$H = \sum_m \left[\omega_c \left(a_m^\dagger a_m + \frac{1}{2} \right) + \frac{\omega_{a, m} \sigma_m^z}{2} \right] + \sum_{\langle l, m \rangle} J_{l, m} a_l^\dagger a_m + \sum_m g_m (a_m^\dagger \sigma_m^- + \sigma_m^+ a_m), \quad (5)$$

where g_m is the atom-photon coupling rate (i.e. vacuum Rabi frequency), and the σ_m^i are the standard Pauli operators. To second order in g_m/Δ_m , the state of the atom induces an a.c. Stark shift of the cavity by $\chi_m = g_m^2/\Delta_m$ [41]. Equivalently, a flip of the atom's state shifts the resonance of the cavity by $2\chi_m$, meaning that any photons remaining in the cavity will have acquired an extra energy of $2\chi_m$. Averaged over many Rabi-oscillations, this shifts the cavity photon frequency by χ_m when two photons are on the same site, causing a faster phase evolution rate than for a single photon. This is equivalent to the effect of an energy cost for two photons on the same site. Thus, by tuning g_m and ω_m , we have enough degrees of freedom to obtain analogous dynamics to those of Eq. 1, having both distinct on-site energies and a tunable nonlinear interaction.

Of particular note, the inclusion of a two-level atom provides a powerful advantage over both cold atom systems and the aforementioned nonlinear-Kerr cavities. As has been experimentally demonstrated [41], due to the commutation of the a.c. Stark shift with the photonic and atomic states, it is possible to perform a quantum non-demolition measurement on the state of the atom (photons) on a given site without affecting the photons (atom) on that site or any other states in the system. Potentially, this could be used to monitor or tune the operation of gates in situ or as part of an error correction scheme.

Finally, we note that while we have focused on the capabilities of superconducting systems in this section, devices based on quantum dots or graphene may offer similar opportunities at optical frequencies [31–37].

Conclusions — We have shown how quantum logic gates can be realized with high fidelity using the quantum walk of ultra-cold atoms on a one-dimensional lattice under experimentally achievable constraints. In particular, we gave a design for a high fidelity CNOT gate along with exact descriptions of single-qubit rotations, a computationally complete set. Additionally, we demonstrated the compilation of a higher-order gate operation into a single operation. Our approach carries several important advantages over previous schemes. First, due to the dual-rail encoding we employ, the states of the system can be prepared and measured by simply placing and detecting single atoms at certain positions, both of

which are straightforward in present experimental systems [17]. Second, each quantum operation is carried out by a single, one-dimensional, time-invariant lattice potential. Third, the devices we propose are compact lattices of size $2n$ (where n is the number of qubits) that can be realized on a line of potential wells with only nearest-neighbor hopping, in agreement with experimental capabilities. Our analysis shows that similar effects could be achieved in certain nonlinear quantum-optical systems.

Acknowledgments — We acknowledge helpful discussions with Terry Orlando, William Oliver and Markus Greiner's group. G.R.S. was supported by the Department of Defense (DoD) through the National Defense Science & Engineering Graduate Fellowship (NDSEG) Program. D.E. acknowledges support from the Sloan Research Fellowship in Physics. Y.L. acknowledges support from the Pappalardo Fellowship in Physics.

* Electronic address: lahini@mit.edu

- [1] Y. Aharonov, L. Davidovich, and N. Zagury, Phys. Rev. A **48**, 1687 (1993).
- [2] E. Farhi and S. Gutmann, Phys. Rev. A **58**, 915 (1998).
- [3] J. Kempe, Contemporary Physics **44**, 307 (2003).
- [4] Salvador Elias Venegas-Andraca, Quantum Information Processing **11**, 1015 (2012).
- [5] B. Do, M. L. Stohler, S. Balasubramanian, D. S. Elliott, C. Eash, E. Fischbach, M. A. Fischbach, A. Mills, and B. Zwickl, J. Opt. Soc. Am. B **22**, 499 (2005).
- [6] H. B. Perets, Y. Lahini, F. Pozzi, M. Sorel, R. Morandotti, and Y. Silberberg, Phys. Rev. Lett. **100**, 170506 (2008).
- [7] Y. Bromberg, Y. Lahini, R. Morandotti, and Y. Silberberg, Phys. Rev. Lett. **102**, 253904 (2009).
- [8] A. Peruzzo, M. Lobino, J. C. F. Matthews, N. Matsuda, A. Politi, K. Poulios, X.-Q. Zhou, Y. Lahini, N. Ismail, K. Worhoff, et al., Science **329**, 1500 (2010).
- [9] M. A. Broome, A. Fedrizzi, B. P. Lanyon, I. Kassal, A. Aspuru-Guzik, and A. G. White, Phys. Rev. Lett. **104**, 153602 (2010).
- [10] A. Schreiber, K. N. Cassemiro, V. Potocek, A. Gabris, P. J. Mosley, E. Andersson, I. Jex, and C. Silberhorn, Phys. Rev. Lett. **104**, 050502 (2010).
- [11] A. Regensburger, C. Bersch, B. Hinrichs, G. Onishchukov, A. Schreiber, C. Silberhorn, and U. Peschel, Phys. Rev. Lett. **107**, 233902 (2011).
- [12] P. P. Rohde, A. Schreiber, M. Stefanak, I. Jex, and C. Silberhorn, New Journal of Physics **13**, 013001 (2011).
- [13] H. Schmitz, R. Matjeschk, C. Schneider, J. Glueckert, M. Enderlein, T. Huber, and T. Schaetz, Phys. Rev. Lett. **103**, 090504 (2009).
- [14] F. Zahringer, G. Kirchmair, R. Gerritsma, E. Solano, R. Blatt, and C. F. Roos, Phys. Rev. Lett. **104**, 100503 (2010).
- [15] C. Weitenberg, M. Endres, J. F. Sherson, M. Cheneau, P. Schaus, T. Fukuhara, I. Bloch, and S. Kuhr, Nature **471**, 319 (2011).
- [16] T. Fukuhara, P. Schaus, M. Endres, S. Hild, M. Cheneau, I. Bloch, and C. Gross, Nature **502**, 76 (2013).
- [17] P. M. Preiss, R. Ma, M. E. Tai, A. Lukin, M. Rispoli, P. Zupancic, Y. Lahini, R. Islam, and M. Greiner, ArXiv e-prints (2014), 1409.3100.
- [18] Y. Lahini, M. Verbin, S. D. Huber, Y. Bromberg, R. Pugatch, and Y. Silberberg, Phys. Rev. A **86**, 011603 (2012).
- [19] A. M. Childs, D. Gosset, and Z. Webb, Science **339**, 791 (2013).
- [20] M. S. Underwood and D. L. Feder, Phys. Rev. A **85**, 052314 (2012).
- [21] D. Aharonov, D. Gottesman, S. Irani, and J. Kempe, Communications in Mathematical Physics **287**, 41 (2009).
- [22] B. A. Chase and A. J. Landahl, arXiv:1011.3245 [quant-ph] (2008).
- [23] D. Nagaj and P. Wocjan, Phys. Rev. A **78**, 032311 (2008).
- [24] M. A. Nielsen and I. L. Chuang, *Quantum computation and quantum information* (Cambridge University Press, Cambridge; New York, 2000).
- [25] S. G. Johnson, *The NLOpt nonlinear-optimization package*, <http://ab-initio.mit.edu/nlopt>.
- [26] A. Rinnooy Kan and G. Timmer, Mathematical Programming **39**, 27 (1987).
- [27] A. Rinnooy Kan and G. Timmer, Mathematical Programming **39**, 57 (1987).
- [28] M. Powell, Tech. Rep., Center for Mathematical Sciences (2009), "NA2009/06".
- [29] D. Deutsch and R. Jozsa, Proceedings of the Royal Society of London. Series A: Mathematical and Physical Sciences **439**, 553 (1992).
- [30] P. Adhikari, M. Hafezi, and J. M. Taylor, Phys. Rev. Lett. **110**, 060503 (2013).
- [31] O. Firstenberg, T. Peyronel, Q.-Y. Liang, A. V. Gorshkov, M. D. Lukin, and V. Vuletic, Nature **502**, 71 (2013).
- [32] M. Gullans, D. E. Chang, F. H. L. Koppens, F. J. G. de Abajo, and M. D. Lukin, Physical Review Letters **111** (2013).
- [33] B. Dayan, A. S. Parkins, T. Aoki, E. P. Ostby, K. J. Vahala, and H. J. Kimble, Science **319**, 1062 (2008).
- [34] D. Englund, A. Faraon, I. Fushman, N. Stoltz, P. Petroff, and J. Vuckovic, Nature **450**, 857 (2007).
- [35] D. Englund, A. Majumdar, M. Bajcsy, A. Faraon, P. Petroff, and J. Vučković, Physical review letters **108**, 093604 (2012).
- [36] R. Bose, D. Sridharan, H. Kim, G. S. Solomon, and E. Waks, Phys. Rev. Lett. **108**, 227402 (2012).
- [37] T. Volz, A. Reinhard, M. Winger, A. Badolato, K. J. Hennessy, E. L. Hu, and A. Imamoglu, Nature Photonics **6**, 605 (2012).
- [38] G. Kirchmair, B. Vlastakis, Z. Leghtas, S. E. Nigg, H. Paik, E. Ginossar, M. Mirrahimi, L. Frunzio, S. Girvin, and R. Schoelkopf, Nature **495**, 205 (2013).
- [39] A. Gangat, I. McCulloch, and G. Milburn, Phys. Rev. X **3**, 031009 (2013).
- [40] A. Blais, R.-S. Huang, A. Wallraff, S. Girvin, and R. J. Schoelkopf, Physical Review A **69**, 062320 (2004).
- [41] D. Schuster, A. Houck, J. Schreier, A. Wallraff, J. Gambetta, A. Blais, L. Frunzio, J. Majer, B. Johnson, M. Devoret, et al., Nature **445**, 515 (2007).

Supplementary Information: Quantum Logic with Interacting Bosons in 1D

Single-qubit gates - To complement the presentation of a controlled-not (CNOT) gate in the main paper, we present the exact construction for a set of single-qubit gates that, together with the CNOT gate, make a universal quantum gate set. Since these are one-qubit operations, they are implemented using one particle in two lattice sites. As such, the interaction (Γ) is irrelevant and the matrix of lattice parameters

$$G = \begin{pmatrix} E_1 & J_{12} \\ J_{12} & E_2 \end{pmatrix}$$

(with $J_{12} \leq 0$) can be directly interpreted as the Hamiltonian governing the single particle. The unitary gate, obtained by evolving with G for a time T , is then $U = e^{-iGT}$.

One simple universal quantum gate set includes the Hadamard gate, the phase-shift gate, and the controlled-NOT (CNOT) gate [S1]. The phase-shift gate is the simplest to implement. It is composed of two decoupled lattice sites in which the on-site energy between the sites is detuned. Specifically, to implement the single-qubit phase-shift operator $R_\theta = \begin{pmatrix} 1 & 0 \\ 0 & e^{i\theta} \end{pmatrix}$, one may apply the single-qubit Hamiltonian

$$G_{R_\theta} = \begin{pmatrix} 0 & 0 \\ 0 & -\theta \end{pmatrix} \quad (\text{S1})$$

for time $T = 1$. (Obviously a different value for T may be chosen, so long as TG_{R_θ} remains the same.) Next in complexity is the single-qubit Hadamard gate $H = \frac{1}{\sqrt{2}} \begin{pmatrix} 1 & 1 \\ 1 & -1 \end{pmatrix}$. The Hamiltonian and propagation time that generates the Hadamard transformation can be solved analytically, and is given by

$$G_H = \begin{pmatrix} \sqrt{2}-1 & -1 \\ -1 & \sqrt{2}+1 \end{pmatrix}, \quad T = \frac{\pi}{2\sqrt{2}}. \quad (\text{S2})$$

Note that a simple tunnelling between two identical wells for half the tunnelling time (analogous to the beamsplitter operation in linear optics) will not reproduce the Hadamard gate in this case. Unlike the bulk quantum optics situation, in which the optical beamsplitter can be asymmetric in phase and thus can reproduce the Hadamard gate exactly, under our Hamiltonian dynamics the splitting is symmetric in phase and therefore modified tunnelling rates and additional diagonal terms are required in order to correct the output phases. We note this holds true also for integrated quantum photonics gates [S2]. A summary of the physical construction for the single-qubit operations is given in Fig. S1.

Alternatively, one can use the (exactly) universal gate set of CNOT together with all single-qubit unitaries. Any single-qubit unitary, U , can be implemented by first decomposing it in the form [S1]

$$U = e^{i\alpha} R_z(\beta) R_x(\gamma) R_z(\delta) = e^{i\alpha} R_z(\beta) H R_z(\gamma) H R_z(\delta)$$

where the z -rotation $R_z(\theta) = \begin{pmatrix} e^{-i\theta/2} & 0 \\ 0 & e^{i\theta/2} \end{pmatrix}$ can be implemented with the Hamiltonian

$$G_{R_z(\theta)} = \begin{pmatrix} 1 & 0 \\ 0 & -1 \end{pmatrix}, \quad T = \frac{\theta}{2},$$

and the x -rotation $R_x(\theta) = \exp \begin{pmatrix} 0 & -i\theta/2 \\ -i\theta/2 & 0 \end{pmatrix}$ can be implemented either with the Hamiltonian

$$G_{R_x(\theta)} = \begin{pmatrix} 0 & -1 \\ -1 & 0 \end{pmatrix}, \quad T = \frac{4\pi - \theta}{2} \quad (\text{S3})$$

or by conjugating $R_z(\theta)$ by the Hadamard operation H described earlier. The phase $e^{i\alpha}$ can be implemented with $G_\alpha = -\alpha \begin{pmatrix} 1 & 0 \\ 0 & 1 \end{pmatrix}$, $T = 1$.

Quantum process tomography for CNOT - The basic idea of quantum process tomography [S3] is to completely determine the mathematical structure of a given operation (in our case, the CNOT on two qubits), by applying the operation to a variety of different input states and measuring each of the resulting states in a variety of bases.

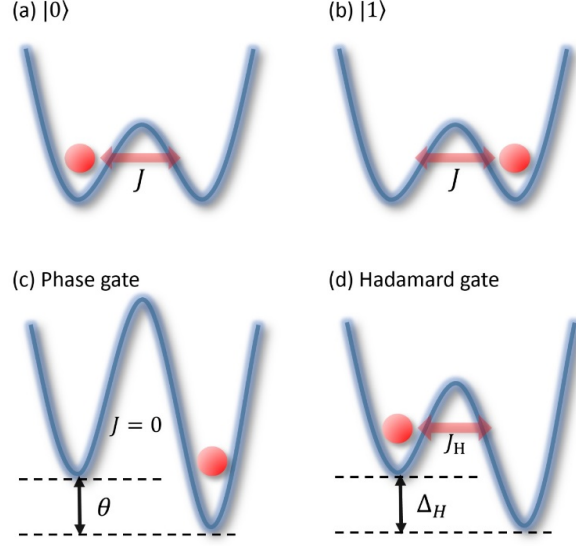


Figure S1: (color online). A double potential well containing a single-boson configuration representing a single qubit in the (a) $|0\rangle$ state and the (b) $|1\rangle$ state. (c) An implementation of the single-qubit phase gate, according to the recipe in Eq. S1. (d) An implementation of the Hadamard gate, according to the recipe in Eq. S2.

Tomography procedures allow much freedom in choosing input states and measurement bases. We want to make such choices wisely to facilitate performing the procedure on our particular experimental apparatus. Two main points guide these choices. One is that the only two-qubit gate be the purported CNOT gate itself — all other gates required for the tomography should be relatively simple so that we adequately assess the CNOT as the major source of errors. The second is that the other gates be easy for the Bose-Hubbard model to implement, preferably with as few gates as possible (since limitations in coherency times may limit the number of gates reasonably performed using current technology). Here we suggest input states and measurement bases to accomplish these goals, requiring only two single-qubit Bose-Hubbard Hamiltonians (one prior to the CNOT, and one following it) per (computational) measurement. Specifically, each measurement in the tomography involves applying an operation of the form $(V_3 \otimes V_4)$ CNOT $(V_1 \otimes V_2)$ to a computational basis state, followed by a measurement in the computational basis, where each V_i can be performed with a single one-qubit Bose-Hubbard Hamiltonian; we therefore need only keep the state coherent for three consecutive operations.

We assume that the reader is following the quantum process tomography procedure outlined in Ref. [S1], which requires measuring Pauli observables. To measure a Pauli matrix $\sigma \in \{I, X, Y, Z\}$, one must perform a basis-transformation gate to their output state so as to measure in the eigenbasis of σ . For $\sigma = I$ and Z , this is trivial, as the computational basis suffices; however, for $\sigma = X$ and Y , we recommend measuring in the following eigenbases, which can be performed by first applying the following basis-transformation matrices,

$$X : \left\{ \frac{1}{\sqrt{2}} \begin{pmatrix} 1 \\ 1 \end{pmatrix}, \frac{1}{\sqrt{2}} \begin{pmatrix} 1 \\ -1 \end{pmatrix} \right\}, \quad U_X = \frac{1}{\sqrt{2}} \begin{pmatrix} 1 & 1 \\ 1 & -1 \end{pmatrix} \quad (\text{S4})$$

and

$$Y : \left\{ \frac{1}{\sqrt{2}} \begin{pmatrix} 1 \\ i \end{pmatrix}, \frac{1}{\sqrt{2}} \begin{pmatrix} 1 \\ -i \end{pmatrix} \right\}, \quad U_Y = \frac{1}{\sqrt{2}} \begin{pmatrix} 1 & -i \\ -i & 1 \end{pmatrix}. \quad (\text{S5})$$

Observe that U_X is the Hadamard matrix, the Hamiltonian for which was given in Eq. S2, and that $U_Y = R_x(\pi/2)$, which is generated by the Hamiltonian in Eq. S3 with $\theta = \pi/2$. Note that for Y we chose a non-standard orthonormal eigenbasis so that the basis-transformation can be accomplished using a single Bose-Hubbard gate.

The input states required to perform the quantum process tomography procedure of Ref. [S1] are straightforward to produce. For example, one may use tensor products of the following single-qubit input states: the computational basis states $|0\rangle$ and $|1\rangle$, the $+1$ X -eigenvector $|+\rangle = U_X|0\rangle = \frac{1}{\sqrt{2}} \begin{pmatrix} 1 \\ 1 \end{pmatrix}$, and the $+1$ Y -eigenvector $|-\rangle = U_Y^\dagger|0\rangle = \frac{1}{\sqrt{2}} \begin{pmatrix} 1 \\ i \end{pmatrix}$,

where U_X and U_Y are given in Eqs. (S4) and (S5). Note that $U_Y^\dagger = R_x(7\pi/2)$ can be generated by the Hamiltonian in Eq. S3 with $\theta = 7\pi/2$.

Computational Methods - In this section, we detail the numerical methods used to find the gates presented in the main paper. We made extensive use of a free-software implementation of a variety of numerical optimization algorithms [S4]. This enabled us to, with a single specification of cost function and constraints, compare the success and computational cost of a number of different optimization approaches. We discovered that a randomly-seeded global optimization algorithm [S5, S6] combined with a gradient-free local algorithm [S7] gave the best performance, both in terms of number of iterations and computational run-time.

Careful selection of the cost function was crucial to the success of this work, and interacted with the choice of the aforementioned algorithms, particularly the local optimizer. Throughout the paper, we define the fidelity of the gate in terms of the Hilbert-Schmidt inner-product between the target unitary gate operation U_0 and the unitary operation U generated by the Hamiltonian at a given step of the optimization (restricted to the logical subspace). Specifically, the fidelity is defined to be

$$F(U_0, U) = |\langle U_0, U \rangle_C|$$

with

$$\langle U_0, U \rangle_C = \frac{\text{Tr}(U_0^\dagger U)}{N},$$

where N is the dimension of the logical space (4 for two-qubit gates). This fidelity can be interpreted as a sort of lower-bound average fidelity of the gate.

To be specific about the iterative numerical process, at each step we generated U from a vector corresponding to lattice parameters and calculated $F(U_0, U)$. Numerically, we found that minimizing the function $1 - F^2$, rather than $1 - F$, gave superior performance. In the case of the algorithm given in Ref. [S7], the reason for this is clear: the algorithm assumes a quadratic cost function. However, we found that even with algorithms designed for linear cost functions (e.g. [S8]), convergence was much slower than for the quadratic cost function.

Finally, in order to ensure that U has the same global phase as U_0 (this is for aesthetic purposes, as $F(U_0, U)$ is invariant under multiplication by a global phase), we placed a cost on the phase of the matrix element $u_{1,1}$. We found this to be most efficiently implemented by adding the term $\sin(\arg(u_{1,1}))^2$ to the cost function. This function is quadratic when perturbed about zero, is non-negative, and is symmetric about $n\pi$ for all $n \in \mathbb{Z}$, making it an ideal candidate function. We verified that the introduction of this additional cost both yielded a U with appropriate phase (see Fig. 2 in the main text) and did not result in a decreased fidelity compared to optimization without this constraint.

* Electronic address: lahini@mit.edu

- [S1] M. A. Nielsen and I. L. Chuang, *Quantum computation and quantum information* (Cambridge University Press, Cambridge; New York, 2000).
- [S2] A. Politi, M. J. Cryan, J. G. Rarity, S. Yu, and J. L. O'Brien, *Science* **320**, 646 (2008), PMID: 18369104.
- [S3] I. L. Chuang and M. A. Nielsen, *Journal of Modern Optics* **44**, 2455 (1997), URL <http://www.tandfonline.com/doi/abs/10.1080/09500349708231894>.
- [S4] S. G. Johnson, *The NLOpt nonlinear-optimization package*, <http://ab-initio.mit.edu/nlopt>.
- [S5] A. Rinnooy Kan and G. Timmer, *Mathematical Programming* **39**, 27 (1987), ISSN 0025-5610, URL <http://dx.doi.org/10.1007/BF02592070>.
- [S6] A. Rinnooy Kan and G. Timmer, *Mathematical Programming* **39**, 57 (1987), ISSN 0025-5610, URL <http://dx.doi.org/10.1007/BF02592071>.
- [S7] M. Powell, Tech. Rep., Center for Mathematical Sciences (2009), "NA2009/06".
- [S8] M. J. D. Powell, *Acta Numerica* **7**, 287 (1998), ISSN 1474-0508, URL http://journals.cambridge.org/article_S0962492900002841.